Thermal and athermal three-dimensional swarms of self-propelled particles

Nguyen H. P. Nguyen,[1] Eric Jankowski,[2] and Sharon C. Glotzer[2,3,4,*]

[1]*Department of Mechanical Engineering, University of Michigan, Ann Arbor, Michigan 48109, USA*

[2]*Department of Chemical Engineering, University of Michigan, Ann Arbor, Michigan 48109, USA*

[3]*Department of Materials Science and Engineering, University of Michigan, Ann Arbor, Michigan 48109, USA*

[4]*Applied Physics Program, University of Michigan, Ann Arbor, Michigan 48109, USA*

(Received 30 December 2011; revised manuscript received 7 June 2012; published 30 July 2012)

Swarms of self-propelled particles exhibit complex behavior that can arise from simple models, with large changes in swarm behavior resulting from small changes in model parameters. We investigate the steady-state swarms formed by self-propelled Morse particles in three dimensions using molecular dynamics simulations optimized for graphics processing units. We find a variety of swarms of different overall shape assemble spontaneously and that for certain Morse potential parameters at most two competing structures are observed. We report a rich "phase diagram" of athermal swarm structures observed across a broad range of interaction parameters. Unlike the structures formed in equilibrium self-assembly, we find that the probability of forming a self-propelled swarm can be biased by the choice of initial conditions. We investigate how thermal noise influences swarm formation and demonstrate ways it can be exploited to reconfigure one swarm into another. Our findings validate and extend previous observations of self-propelled Morse swarms and highlight open questions for predictive theories of nonequilibrium self-assembly.

DOI: 10.1103/PhysRevE.86.011136 PACS number(s): 05.90.+m, 05.10.−a, 89.75.Kd

I. INTRODUCTION

The emergence of ordered swarms from a collection of autonomous self-propelled agents is a ubiquitous natural phenomenon. In biology, swarming is a common feature of social organisms, and flocks of birds, schools of fish, and herds of buffalo have been described by simple models [1–5]. Nonbiological systems of self-propelled particles, including rotating magnetic disks [6] and microdiodes [7], also exhibit of steady-state swarms [4,8–11], and recent work has elucidated many ways the interactions between particles can influence swarm structure [1,12–24], primarily in two dimensions.

Understanding how the interactions between agents results in swarms of a particular shape has a wide range of applications, including the distributed control of unmanned vehicles [24], assembly of mobile sensor networks [25], and microscale mixing [7]. Interaction potentials that are qualitatively similar to the potentials that describe nanoparticle interactions but scaled to larger lengths have been utilized to control and reconfigure mobile vehicles flocks that would otherwise require complex and costly centralized control systems to achieve the same task [24,25]. Self-propelled microsensors powered by alternating electric fields have demonstrated mixing within microchannels [7]. Creating a swarm that performs a preprogrammed task, whether within a microchip or between cities, depends on our ability to robustly control the structure of a swarm through the manipulation of the interactions between agents.

One interparticle interaction that has received considerable attention is the generalized Morse potential, first introduced for modeling swarms by Levine *et al*. [14]. In two dimensions, D'Orsogna *et al*. [16] discovered rings, vortex-like swarms, and circular clumps in systems of self-propelled particles interacting via a Morse potential and showed how the swarm stability varies with swarm size. The Morse potential has been used to demonstrate the control of swarming vehicles [24] and in three dimensions was used to model systems of toroidal swarms whose translational motion was tuned with thermal noise [26]. The structural diversity observed for two-dimensional (2D) Morse swarms is impressive, and it is natural to ask what other sorts of three-dimensional (3D) swarms might be stable and how robust their stability is to thermal fluctuations. Unfortunately, no predictive theory for swarm stability currently exists, and the parameter space from which 3D Morse swarms can be chosen is enormous. With four Morse parameters and three independent thermodynamic parameters (volume, particle number, and temperature), we rely on computer simulations as the primary tool for predicting the conditions under which swarms are stable, and the structural and dynamical character of potentially achievable swarms.

Here we perform computer simulations of self-propelled Morse particles using graphics processing unit (GPU) optimized software [27] to explore the formation of 3D stable swarms in both thermal and athermal environments and gain insights on their dynamics and stability. Our simulation code allows for sampling of vast regions of parameter space where we observe swarms including tori, hollow shells, and two-dimensional rings. The "phase diagram" we report as a function of Morse potential parameters is richly diverse, with large regions where one swarm is stable over all others, but other regions where swarms are observed over only narrow parameter ranges. We observe notable deviations from equilibrium pattern formation in this far-from-equilibrium system, including assembly of competing swarms at a given state point, and we demonstrate that initial conditions can be chosen to bias the formation of one structure over another. We observe that thermal noise can influence the stability of one structure over another, and we demonstrate how noise can be used to reproducibly and repeatedly switch between different swarms. Beyond these new findings, our work highlights the

*sglotzer@umich.edu

need for efficient computational tools and predictive analytical techniques for the study of swarm formation, and demonstrates the precise control over swarm morphology that can be accomplished with a model system.

This paper is organized as follows. In Sec. II we describe the pairwise interaction parameters and "active" particles that define our model, the methods we employ to perform simulations on GPUs, and the quantities we calculate to characterize swarms and their structure. In Sec. III we present the results of our extensive simulations. These results include a "phase diagram" that summarizes the swarms we find in the absence of thermal noise, two case studies for structural transitions induced by thermal noise, and an evaluation of swarm structure sensitivity to initial conditions. In Sec. IV we discuss similarities and differences of the swarm self-assembly as compared to equilibrium self-assembly. In Sec. V we conclude with a summary of our work and highlight future possible extensions.

II. MODEL AND METHOD

A. Model

We consider particles interacting via the generalized two-body Morse potential [14]

$$U(r_{ij}) = C_r \exp\left(\frac{-r_{ij}}{l_r}\right) - C_a \exp\left(\frac{-r_{ij}}{l_a}\right), \qquad (1)$$

where r_{ij} is the distance between two particles i and j, C_a is the attraction strength, C_r is the repulsion strength, l_a is the attraction length scale, and l_r is the repulsion length scale. These parameters can be chosen to model a wide range of interaction types, from purely repulsive and/or long-range attractive, to particles that can overlap but have an energetic barrier to doing so. To model the motion of self-propelled Morse particles in a thermal bath, we update particle positions using the Langevin equation of motion [28]

$$m_i \frac{\partial \vec{v}_i}{\partial t} = \vec{F}_i^C + \vec{F}_i^R + \vec{F}_i^D. \qquad (2)$$

Here m_i and v_i are the mass and velocity of particle i, t is time, and $\vec{F}_i^C$, $\vec{F}_i^R$, and $\vec{F}_i^D$ represent the conservative, random, and drag forces, respectively. The conservative force between two particles is the usual negative gradient of the potential summed over all neighbors:

$$\vec{F}_i^C = \sum_{i \neq j} -\nabla U(r_{ij}). \qquad (3)$$

The random force and drag force are related through the fluctuation-dissipation theorem,

$$\left\langle \vec{F}_i^R \right\rangle = 0, \qquad (4)$$

$$\left\langle \vec{F}_i^R(t) \vec{F}_i^R(t') \right\rangle = 6\gamma T^* \delta_{ij} \delta(t - t'), \qquad (5)$$

where γ is proportional to fluid viscosity, T^* is the dimensionless temperature, δ_{ij} is the Kronecker delta function, and $\delta(t)$ is the Dirac delta function. We model particle self-propulsion as in Refs. [16,26] with a modified drag force

$$\vec{F}_i^D = (\alpha - \gamma - \beta |\vec{v}_i|^2) \vec{v}_i, \qquad (6)$$

where $\alpha - \gamma$ determines the net propulsion strength and β determines the amplitude of the nonlinear drag force. The propulsion and drag forces act parallel to a particle's velocity vector and define an optimal velocity $v^* = \sqrt{\frac{\alpha - \gamma}{\beta}}$ towards which particles are driven.

B. Method

We implement the above model in HOOMD-blue, an open-source GPU-based Molecular Dynamics package developed by our group, which we have extended with packages for calculating and applying self-propulsion forces and the Morse potential via CUDA kernels executed on NVIDIA Tesla S1070 graphics cards [27]. The Morse potential Eq. (1) is truncated and shifted to zero at $r_{ij} = 5\sigma$, which avoids the potential energy drift that can occur with an unshifted potential. We employ generic units of distance σ, particle mass m, and energy ϵ. The Morse potential energy at $r_{ij} = 0$ is equal to 1ϵ for $C_r = 2$, $C_a = 1$, $l_r = 1$, $l_a = 1$. The "temperature" of the system is a thermal energy related to real temperature by $T^* = k_B T_{\text{real}}$ in units of ϵ. The value of k_B is uniquely determined by the choice of real units for energy, distance, and mass. The time unit τ is derived from $\tau = \sqrt{\frac{m\sigma^2}{\epsilon}}$. We update particle velocities and positions using the two-step velocity Verlet integration scheme [29] with $dt = 0.001$ or 0.005. Generally we find $dt = 0.005$ to be sufficiently small for reliable integration of the Langevin equation, except for very low values of C and large values of l, where swarm artifacts can appear for $dt > 0.002$. For $N = 600$ point particles in a 20σ cubic simulation box with periodic boundary conditions, a simulation of 2×10^6 time steps with $dt = 0.005$ requires about an hour on a single GPU. The 4000 simulations required to create Fig. 2 were completed in three days and would have required two to three months if performed with LAMMPS [30,31] on a parallel CPU cluster.

A typical trial run begins with $N = 600$ particles initialized randomly within a 5σ cubic region (cell) centered within the larger 20σ cubic simulation box. Initializing particles within the 5σ cell ensures one swarm is formed from all particles and avoids finite-size effects that could be imposed by having a simulation volume commensurate with the interaction potential length scale. Each component of the particle velocities are initialized randomly from a Gaussian distribution with mean $T^* = 1.0$ and standard deviation $\delta T^* = 1.0$. Henceforth, when we refer to "random initial velocities" we mean they are drawn from this distribution. We typically set $\alpha = 2.0$, $\gamma = 1.0$, and $\beta = 0.5$, and perform 2×10^6 time steps with a step size of $dt = 0.005$. Simulation runs that differ from these initial conditions are noted and explained. Different system densities result in the same overall swarm morphologies at a given state point, but where the number of swarms observed per simulation and the size of a given swarm can vary from run to run.

The simulation times of 2×10^6 time steps are chosen to allow for sufficient sampling of steady-state structures after transient swarms die out. Generally we find that transients have disappeared after 1×10^6 time steps. We define a steady-state swarm for a simulation run if there exists a structure or collection of structures that persist over the final 1×10^6 time steps with a well-defined average and standard deviation

for their total energy. We distinguish among different swarms by calculating relative eigenvalues of their moment of inertia tensors and comparing them with the corresponding values that are characteristic to symmetric, circular structures such as spherical shells and rings. If the values match within an allowable tolerance of 10%, the structure is identified as a swarm.

To distinguish between swarms where particles travel about a fixed central point [e.g., a shell; Fig. 1(b)] and swarms where particles travel about a fixed central axis [e.g., a ring; Fig. 1(c)] we define the alignment order relative to particle i:

$$A_i = 2\left(\frac{\sum_{j=1}^{N}|\vec{M}_i\cdot\vec{M}_j|}{\sum_{j=1}^{N}|\vec{M}_i||\vec{M}_j|} - 0.5\right), \tag{7}$$

where

$$\vec{M}_i = \vec{r}_i \times \vec{v}_i \tag{8}$$

is the angular momentum for particle i traveling at a velocity v_i located at position r_i relative to its swarm center of mass. In practice we select A to be the maximum value of A_i from the N measurements for a swarm, indicating the correlations in angular momentum about the axis where they are most correlated. When $A = 0$ particles move in circles whose axes have no average correlation, as is the case for the shell [Fig. 1(b)]. When $A = 1.0$ the circular paths traveled by all particles share the same axis, as is the case for the ring [Fig. 1(c)]. In addition to distinguishing between shells and rings, we show that A is useful in characterizing the velocity correlations for the other swarms studied in this work. A metric similar to Eq. (7) is used to distinguish 2D vortices and flocks in Ref. [23].

III. RESULTS AND DISCUSSION

We perform 4000 MD simulations using HOOMD-Blue to determine the athermal steady-state swarms that emerge for Morse particles in three dimensions in Sec. III A. We validate our approach by confirming previously reported swarm behavior from Refs. [16] and [26] and report new swarms and new behaviors including swarm coexistence. In Sec. III B we perform 1760 MD simulations of different initial conditions and find that correlations in angular momentum largely determine the trajectory of a swarm and can influence the steady-state swarm observed in coexistence regions. We perform 950 MD simulations of thermal systems and find random thermal fluctuations can influence structural stability and provide a means to switch between different swarms.

A. 3D swarms

We observe the morphology of 3D Morse swarms depends upon the shape of the interaction potential, as has been demonstrated in detail for 2D systems [14,16,22,23]. We perform 10 independent simulations at each of 400 different combinations of two reduced interacting potential parameters $l = \frac{l_r}{l_a}$ and $C = \frac{C_r}{C_a}$, with $l_r = 1$, $C_r = 1$, and $T^* = 0$. Henceforth when we specify values of C or l without specifying C_a or l_a, we take $C_a = 1$ and $l_a = 1$. Simulations are initialized with $N = 600$ particles randomly distributed in a 5σ cubic region

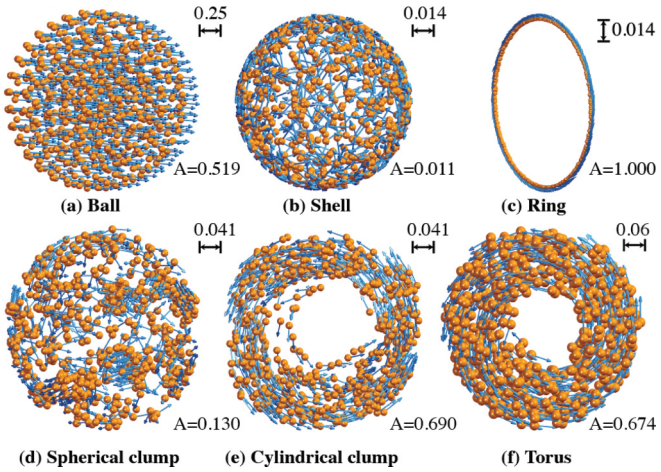

FIG. 1. (Color online) Three-dimensional self-propelled swarms of $N = 600$ Morse particles at $T^* = 0$, $\alpha = 2$, $\gamma = 1$, and $\beta = 0.5$. Steady-state swarms are observed in MD simulations after 2×10^6 time steps have evolved for particles within a 20σ simulation box with periodic boundary conditions. Particles are initialized with random velocities and are randomly distributed within a 5σ cubic region inside the simulation box. Blue arrows indicate particle velocities. Orange spheres represent particle positions, but the sphere diameters to not correspond to particle size. Scale bars are shown in the upper right and alignment order A is shown in the lower left of each swarm. Swarm radii range from 0.06σ to 0.3σ (ball). (a) Ball ($C = 1.5$, $l = 0.5$) composed of concentric spherical layers of particles and identical velocities. (b) Stationary hollow shell ($C = 0.5$, $l = 0.5$) composed of particles that travel in circular orbits. (c) Stationary ring ($C = 0.5$, $l = 0.5$) with all particles traveling in the same circular orbit. (d) Stationary spherical swarm ($C = 0.6$, $l = 0.5$) with clumps of particles that travel in circular orbits. (e) Stationary cylindrical swarm ($C = 0.6$, $l = 0.5$) composed of clumps of particles traveling about the same circular orbit. The particles within the clumps move in a cylindrical fashion, but follow a complex path such that the cross-sectional shape of the cylinder appears to be time dependent. (f) Torus ($C = 0.6$, $l = 0.3$) composed of particles that travel in circular orbits of different radii, but share an axis of rotation. Particle paths within the torus span the entire volume: A particle that is near the hole eventually moves to the outer part and back again. See Supplemental Material videos 1–6 [32] for movies of these swarms.

with random velocities, within a 20σ simulation box with periodic boundary conditions. For most values of l and C in the range $0.1 \leqslant l \leqslant 2.0$ and $0.1 \leqslant C \leqslant 2.0$ we observe one of six distinguishable swarms: balls, shells, rings, spherical clumps, cylindrical clumps, and tori (Fig. 1). We summarize the relationship between observed swarm morphologies and Morse potential parameters in Fig. 2. There are three primary types of observations summarized in the phase diagram; regions where one swarm always self-assembles, regions where two swarms coexist (e.g., "Torus-Ball" and "Shell-Ring"), and regions where no coherent swarms emerge ("Mixture" and "Random" in Fig. 2). In the Random region the repulsion portion of the Morse potential dominates, precluding swarm coalescence. In the Mixture region there is an energy barrier to particle agglomeration, but occasionally small ($N = 2$ to 10) translating clusters appear.

A large portion of Fig. 2 is represented by the ball structure [Fig. 1(a)]. The ball structure is found only for potentials

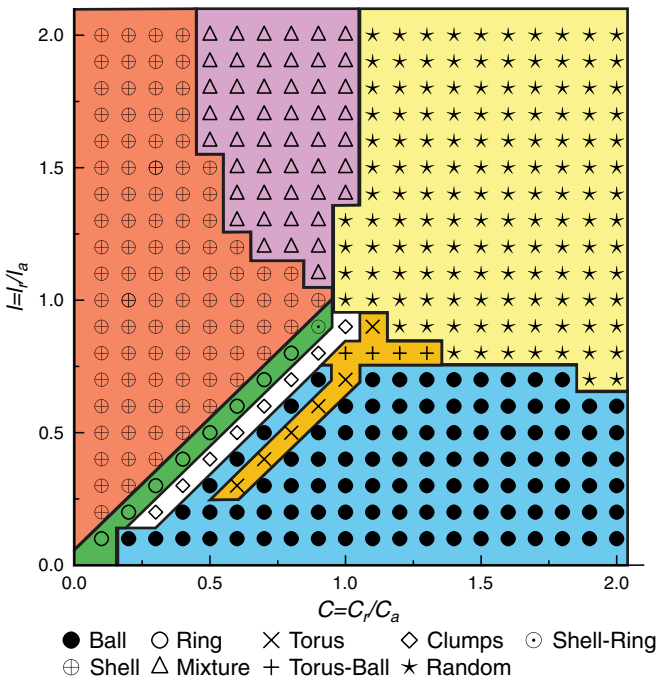

FIG. 2. (Color online) "Phase diagram" for 3D stable structures assembled at values of $0.1 \leqslant l \leqslant 2.0$ and $0.1 \leqslant C \leqslant 2.0$, $T^* = 0$, $\alpha = 2$, $\gamma = 1$, and $\beta = 0.5$. The ratio of repulsion to attraction strength $C = \frac{C_r}{C_a}$ and the ratio of repulsion to attraction length scales $l = \frac{l_r}{l_a}$ determine the shape of the interaction potential and the swarms observed at steady state. In the upper right quadrant ($l > 1$, $C > 1$) repulsion dominates the potential, preventing organized clusters from assembling. In the lower right quadrant ($l < 1, C > 1$) the repulsion is short-ranged and the attraction is long-ranged, resulting in translating spherical balls. In the lower left quadrant ($l < 1$, $C < 1$) attraction dominates the potential and the phase diagram is most complex, with shells, rings, tori, balls, and clumps all stabilized within narrow ranges of l and C. In the top left quadrant ($l > 1$, $C < 1$) particles are attractive, but the repulsive length scale dominates, giving rise to hollow shells.

that are repulsive when particle separation is small and attractive when separation is large, similar to the Lennard-Jones potential. All particles in a steady-state ball travel with an identical linear trajectory with speed $\bar{v}_B = 2.0 \pm 0.0$. The structure of the particles within the ball, concentric spherical shells, is a minimum for the potential energy function (1). Another significant portion of Fig. 2 is represented by the shell swarm [Fig. 1(b)]. The shell swarm is hollow, with individual particles traveling in circular paths on the surface of a sphere and with no correlation between particle orbits. Shells are formed when the attraction between particles is large and have average velocity $\bar{v}_S = 1.993 \pm 0.003$. Between the shell and ball regions of Fig. 2 we finds regions where rings [Fig. 1(c)], clumps [Fig. 1(d) and 1(e)], and tori [Fig. 1(f)] are observed. Rings have average velocity $\bar{v}_R = 1.994 \pm 0.003$ and differ from shells in that all of the particles share an axis of rotation. Tori ($\bar{v}_T = 1.89 \pm 0.410$) differ from rings in that not all particles travel in a circular orbit of the same radius. Cylindrical clumps ($\bar{v}_{CC} = 1.96 \pm 0.28$) are similar to tori, but particles are clumped and not uniformly distributed as they are in the torus. Spherical clumps ($\bar{v}_{SC} = 1.93 \pm 0.36$) are similar to shells in that all particles travel in circular orbits of the same radius, but the particles are not uniformly distributed. The average velocities we report above correspond to the state points indicated in Fig. 1 and, except for the ball swarms, can differ slightly for different state points.

The 3D phase diagram we report in Fig. 2 is qualitatively similar to the 2D phase diagram calculated analytically in D'Orsogna *et al.* [16]. Both phase diagrams have regions of instability in the upper right quadrant and show the richest swarm diversity along the $l/C = 1$ line. We check our implementation reproduces 2D results from Ref. [16] and find the expected swarms at corresponding state points: clumps ($N = 100$, $\alpha = 1.0$, $\beta = 0.5$, $l_r = 0.5$, $l_a = 1$, $C_r = 0.6$, $C_a = 1$), ring clumping ($N = 100, \alpha = 1.0, \beta = 0.5, l_r = 0.5$, $l_a = 1.2$, $C_r = 0.6$, $C_a = 1$), rings ($N = 100$, $\alpha = 1.0$, $\beta = 0.5$, $l_r = 0.5$, $l_a = 1$, $C_r = 0.5$, $C_a = 1$), and vortices ($N = 300, \alpha = 1.0, \beta = 0.5, l_r = 0.5, l_a = 2, C_r = 1.0, C_a = 0.5$). Some of the structures we report here are analogues of the 2D swarms predicted in Refs. [14,16,22,23]. The 3D ball is similar to the 2D coherent flock state reported in Ref. [23], in which particles travel at identical velocities and reside in their potential minima. The 3D hollow spherical shell corresponds to the 2D ring [14,16,22,23], and the 3D spherical clumps are analogous to the circular swarm of clumps in two dimensions [16,23].

We also observe some differences between our 3D swarms and Morse swarms reported in other work. At $C = 1$ and $l = 0.2$, conditions where a vortex is formed in two dimensions, we expect to observe its 3D analog, the torus. In our MD simulations we observe the torus as an initial transient, but find that it eventually transforms into a ball. When not confined to a 2D plane, particles are able to reconfigure into a potential energy minimizing sphere and achieve v^* simultaneously at this state point. These findings are consistent with Strefler *et al.* [26], where transitions between torus and ball swarms are reported when the Morse potential is tuned to have a repulsion at small r_{ij}.

It is not obvious that we should observe 2D rings in our 3D simulations and that they should be stable across many (l,C) values, as seen in Fig. 2. We observe coexistence of shells and rings at $l = 0.9$ and $C = 0.9$, which is interesting because swarm coexistence is not reported in previous Morse swarm work. In a departure from equilibrium statistical mechanics, we find that in the regions of swarm coexistence the probability of forming one swarm can be biased by choice of initial conditions, which we discuss in detail in the following section.

B. Initial conditions

Here we consider three points on the phase diagram and investigate ways in which initial conditions can be chosen to bias swarm formation. First, we show that although swarms may not assemble spontaneously in the Random region of Fig. 2, a preassembled swarm can be maintained there. Second, we show in a region of torus-ball coexistence that swarm formation is not sensitive to initial conditions. Third, we show that while either initial velocity correlations or initial spatial arrangement can bias swarm formation at the shell-ring coexistence point ($l = 0.5$, $C = 0.5$), a metric that combines

these measurements [alignment order A; Eq. (7)] is a good predictor for the final steady state.

At $l = 1.7$ and $C = 1.2$ we observe no ordered structure assembling from particles initialized randomly within a 5σ cubic region centered within a 20σ simulation box with periodic boundary conditions. If we instead initialize particles as a small shell that fits within the attraction region of the potential, we observe that the shell shrinks or expands, depending on its initial size, to another shell that becomes stable for the remainder of 1×10^6 time step simulations. The necessary condition for shell formation is that particles are initialized within the attraction region and have sufficiently low kinetic energy that they will not escape to the repulsive regime of the Morse potential. Indeed, we also find shells stabilized in the Random region by initializing particles on a single point with random initial velocities. By initializing the system as a shell, we find shells are stable within the region ($l = 1.7$, $C \leqslant 1.5$), which spans the Mixture region as well as the Random region.

Next we consider $l = 0.8$ and $C = 1.0$, where the ball and torus coexist in our simulations. We perform simulations initialized as a ball, as a cylinder, and randomly distributed within a 5σ cube, with 100 independent runs with different random initial velocities. At these parameters, we find the probability of observing a toroidal swarm to be 6% for all three initial conditions. In all cases that the torus does not form, a spherical ball forms instead and translates through the simulation box.

Finally, we consider ring and shell coexistence at $l = 0.5$ and $C = 0.5$. We note that whenever we observe a ring, we also observe that it is preceded by a hollow shell which then transforms into a ring. The shell-to-ring transition occurs over 4×10^4 time steps and can occur as many as 4×10^4 time steps after the shell has self-assembled. We perform simulations in which particle positions are initialized as a shell, sphere, cylinder, and randomly distributed within a 5σ cube to investigate sensitivity to initial conditions at this state point. For each initial condition we perform 100 runs with random initial velocities and record the structure observed after 1×10^6 time steps (Fig. 3). When initialized as a shell, only 2% of swarms transition into rings, a substantially lower percentage than the 98% of swarms that form rings from spatially randomized initial conditions, all of which pass through a hollow shell transition state. For each of the 100 runs initialized as a cylinder, all transition into rings. For the runs initialized as balls, 12% transition into rings.

The sensitivity of swarm morphology to initial conditions we report is similar to that reported in Ref. [6], in which magnetic, millimeter-sized disks are driven by an external rotating permanent magnet to self-assemble ordered patterns on a liquid-air interface. A variety of ordered patterns are formed as a result of competing magnetic attraction and hydrodynamics repulsion as the disks spin in the fluid. The authors demonstrate that, depending on initial conditions, a system of one large and nine small disks self-assembles into two different stable configurations. Another similarity between our ring-shell coexistence and the swarm coexistence in Ref. [6] is that swarm size can be increased as self-propulsion is increased. In the system of 10 equally sized disks from

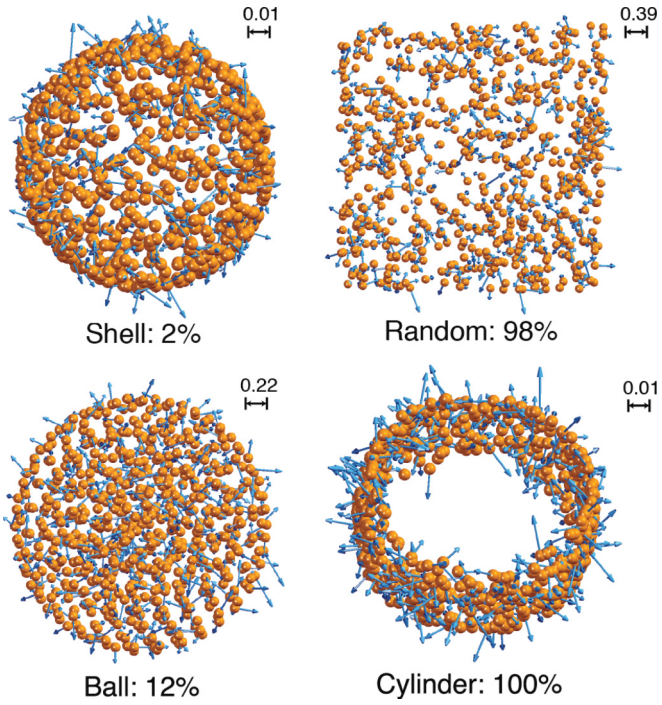

FIG. 3. (Color online) Four initial conditions and their probabilities of transitioning to a ring. The shell and cylinder initial conditions have radii of 0.062. The ball has a radius of 1.35, and the random configuration is distributed randomly in cubic box with side length of 5. Ring transition probabilities are calculated from 100 independent runs performed for each of the indicated initial condition with $T^* = 0$, $\alpha = 1$, $\gamma = 1$, $\beta = 0.5$, $C_r = 0.5$, $l_r = 0.5$, $C_a = 1$, $l_a = 1$, and $N = 600$ with random initial velocities.

Ref. [6], two different ordered patterns can self-assemble and interconvert. While we observe transitions from shells to rings, we never observe the reverse transition. The one-way conversion we observe is interesting because the ring has neither a lower potential energy nor higher entropy than the shell, though the particles are traveling at slightly more constant velocities. The smaller energy dissipation in the ring associated with more constant velocities is consistent with the hypothesis of Grzybowski *et al.* [6] where lower dissipation enhances swarm stability.

We find as a shell transforms into a ring the axes of rotation for the individual particles gradually align, resulting in cylindrical bands, the subsequent alignment of which results in a ring. See Supplemental Material video 3 [32] to view this transition. To investigate the alignment of angular momenta further, we initialize 1000 random shells with random initial velocities and run for 1×10^6 time steps. We record the initial alignment order A and the final steady-state swarm, and summarize the correlation between the two in Fig. 4. The more the particle angular momenta are initially aligned, the higher the probability that the shell would transform to a ring. In particular, Fig. 4 shows that if a shell experiences an instantaneous A greater than 0.15 we would expect it to transition into a ring.

We perform additional simulations with three different spatial initializations and two velocity distributions and observe the initial A trajectories in detail. Simulations are initialized as

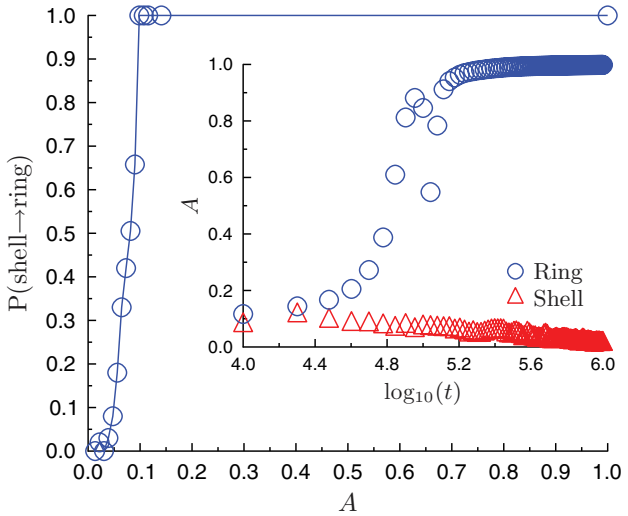

FIG. 4. (Color online) Probability of a random shell transforming into a ring as a function of alignment order A [Eq. (7)] at $T^* = 0$, $\alpha = 1$, $\gamma = 1$, $\beta = 0.5$, $C_r = 0.5$, $l_r = 0.5$, $C_a = 1$, $l_a = 1$, and $N = 600$. The blue line is drawn as a guide to the eye. Inset are representative alignment order trajectories for swarms that form a shell (red triangles) and ring (blue circles).

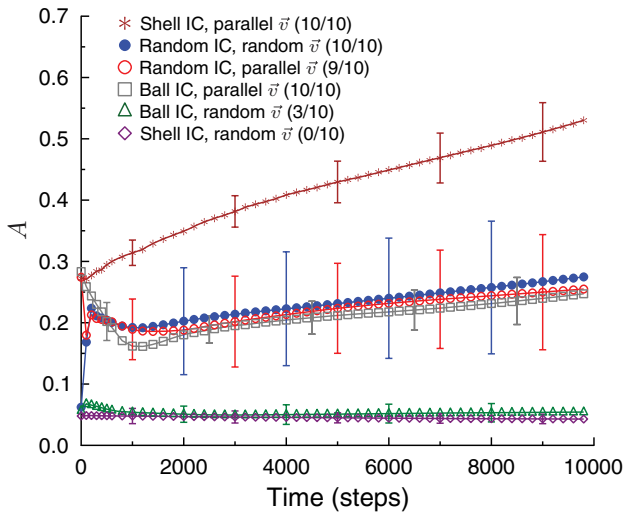

FIG. 5. (Color online) Initial time evolution of the alignment order A averaged over 10 independent runs for six different combinations of initial arrangements and initial velocities. The particles are spatially initialized either randomly within a 5σ cube, within a 2.7σ ball, or on a 0.062σ shell within a 20σ cubic simulation box with periodic boundary conditions. Velocities are initialized from a Gaussian distribution with mean 2 and standard deviation 1 (random $\vec{v}$) or drawn from the ring velocity distribution with mean 2, standard deviation 0.15, and z component = 0 (parallel $\vec{v}$). The number of observed rings after 1×10^6 time steps are shown in parentheses. Error bars are plotted every 2000 steps and denote one standard deviation.

the random, ball, or shell arrangements from Fig. 3 with either a random Gaussian velocities of mean 2 and standard deviation 1, or velocities drawn from a ring swarm (velocities parallel with mean 1.994 and standard deviation 0.003). We then run 10 independent 0.5-million-step simulations for each of the six cases and record the number of rings formed. The average A over initial 1×10^4 step trajectories for these six cases are shown in Fig. 5. We see here that the combined choice of spatial arrangement and velocity distribution determine the initial A trajectory, which can predispose a swarm to give rise to a ring versus a shell. In all cases where the A trajectory has a positive slope after 2000 steps, A increases past 0.15 and rings result. If the initial A trajectory is sufficiently low, as was the case for one random initial condition initialized with velocities from a ring, the A trajectory can begin above 0.15, but dip below and stay below, resulting in a shell. The three instances of Ball initial conditions with random velocities resulting in a ring have slightly positive A slopes that eventually cross $A = 0.15$ after a few hundred thousand steps.

In summary, the sensitivity of steady-state swarm morphology to initial conditions is not uniform across the state space sampled in Fig. 2. In some regions we find swarm formation to be robust to initial conditions, while in others we find both spatial correlations and velocity correlations can have an impact on the rates of swarm formation. For the case of the shell-ring coexistence in particular we find that alignment order A, a metric that combines velocity and spatial correlations in its measurement of angular momentum correlations, provides predictive capabilities between the two competing swarms. The combined choice of initial positions and velocities determine whether A shall increase or decrease initially, and whether this trajectory stabilizes above or below 0.15 determines the proportion of rings observed. In regions where we observe sensitivity to initial conditions, we also expect to observe sensitivity to random noise, which we explore in the next section.

C. Noise

In this subsection we perform simulations at $T^* > 0$ to investigate how thermal fluctuations can influence the formation of swarms. We find in general that for $T^* > 0.20$ the attractive forces between particles are not large enough to stabilize ordered swarms anywhere in the (l, C) range reported in Fig. 2. The highest temperature at which a swarm can be assembled at a particular state point (the order-disorder transition temperature) depends upon the shape of the interaction potential and the initial conditions for self-propelled particles and is an interesting area of future study. Here we focus on the torus and ball, and ring and shell, coexistence regions and find that increasing temperature stabilizes one swarm over the other, as long as T^* is below the order-disorder transition temperature.

At $C_r = 0.9$, $l_r = 0.6$, $C_a = 1$, and $l_a = 1$, a parameter combination at which tori are found, increasing temperature can transform a torus swarm into a swarm shaped like a bumpy sphere. We begin with a preassembled $N = 600$ torus and gradually increase the noise intensity from 0 to 0.08 and then reduce the intensity back to zero with a change of $\delta T^* = 0.01$ every 1 million time steps. We find that when $T^* > 0.03$ the torus transforms into a bumpy sphere, which translates randomly throughout the simulation box. As the noise intensity is reduced to zero, the bumpy sphere transitions back to a torus. This noise-induced transition from stationary swarm to mobile

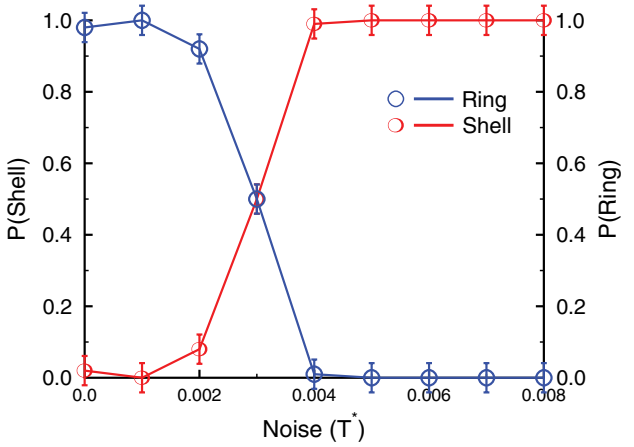

FIG. 6. (Color online) Probability of shell [red (Low curve at small values of noise)] and ring [blue (Upper curve at small values of noise)] formation as a function of T^* at $\alpha = 2$, $\gamma = 1$, $\beta = 0.5$, $C_r = 0.5$, $l_r = 0.5$, $C_a = 1$, $l_a = 1$, and $N = 600$. 100 independent runs are performed at each noise level, with particles initially randomized in a 5σ cube within a 20σ cubic simulation box and are evolved for 1×10^6 time steps. Error bars denote one standard deviation.

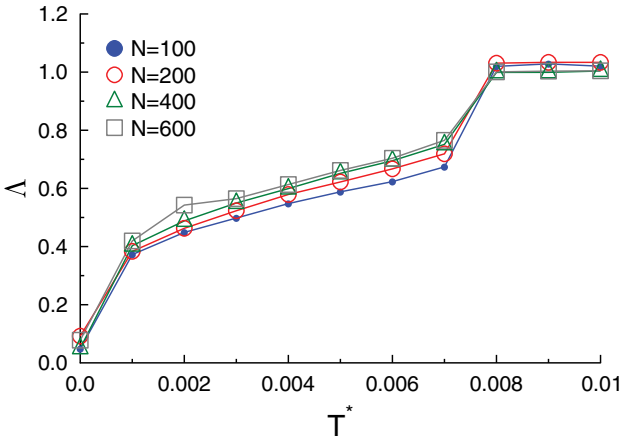

FIG. 7. (Color online) Normalized cylinder height Λ as a function of dimensionless temperature T^* and number of particles N. Particles are initialized as a ring with random velocities. $\alpha = 2$, $\gamma = 1$, $\beta = 0.5$, $C_r = 0.5$, $l_r = 0.5$, $C_a = 1$, and $l_a = 1$. Λ are averaged over 10 simulation snapshots and over 10 independent simulation runs, where the snapshots are the last 10 at 1×10^4 time step increments. The standard deviations of Λ are less than 3% of the mean values and are not shown.

swarm and back again is qualitatively similar to the transition reported in Strefler *et al.* [26]. As in Ref. [26] we find the velocity of the translating bumpy sphere scales with T^*. Our observations of torus stability differ slightly from those of Strefler *et al.*, where stable tori are found at $C_r = C_a = l_r = 0.5$, $l_a = 2$, and $T^* = 0$. At that state point we find the torus always transitions into a ball after 4×10^5 steps.

To investigate the sensitivity of ring and shell formation to thermal fluctuations we perform 100 independent MD simulations at each temperature from $T^* = 0$ to $T^* = 0.008$ at increments of $\delta T^* = 0.001$. Here $\alpha = 2$, $\gamma = 1$, $\beta = 0.5$, $l = 0.5$, and $C = 0.5$. Particles are initialized randomly within a 5σ cubic region within the 20σ simulation box with periodic boundary conditions and simulated for 1×10^6 time steps. We find that the probability of assembling a ring decreases as T^* increases (Fig. 6), undergoing a sharp transition at $T^* = 0.003$, above which shell self-assembly is enhanced.

We also observe the rings formed at $T^* > 0$ are no longer flat, but cylindrical. We perform additional simulations initialized from a ring configuration and ramp temperature from $T^* = 0$ to 0.008 by a step increase in temperature of $\delta T^* = 0.001$ every 1×10^6 time steps, followed by a reverse ramping back to $T^* = 0$, for a total of 16×10^6 time steps. We perform these simulations for swarms of size $N = 100$, $N = 200$, $N = 400$, and $N = 600$ and find that cylinder height increases linearly with T^* from $T^* = 0.001$ to $T^* = 0.007$ (Fig. 7). Furthermore, we find that by normalizing the cylinder height by the cylinder diameter, this trend is independent of swarm size (Fig. 7). When $T^* > 0.007$, cylinders transition into hollow shells. This transition can be used as part of a reversible sequence of steps to convert rings into cylinders into shells and back into rings (Fig. 8). We find that by dropping the temperature from $T^* = 0.008$ to $T^* < 0.007$, a shell will transform into a ring or cylinder (depending on the temperature) if its instantaneous alignment order A is sufficiently large (Fig. 4).

IV. DRIVING FORCES

Swarm formation in self-propelled particles can be considered as a perturbation to equilibrium self-assembly. In the limit that $\alpha \to 0$ and $\beta \to 0$, Eq. (2) becomes the traditional

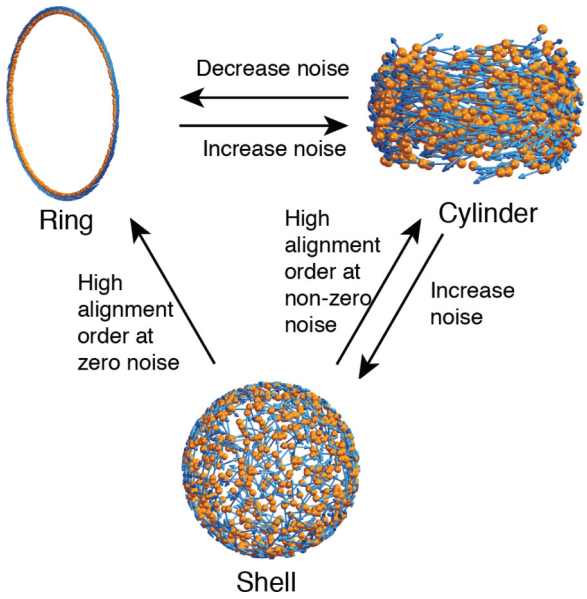

FIG. 8. (Color online) Mechanisms of structural transitions among shells, rings, and cylinders. Increasing the temperature of a ring causes it to transition into a cylinder of increasing height. At large enough T^*, cylinders transition into hollow shells. The transformation of a hollow shell into a cylinder or ring requires not only that the temperature be decreased below $T^* = 0.007$, but also that an instantaneous fluctuation in alignment order is sufficiently large to initiate the transition. The transition involves the shell polarizing into cylindrical bands, which align eventually turning into a cylinder with noise-dependent height or a ring if the noise is zero.

Langevin equation modeling Brownian motion, from which equilibrium distributions of configurations can easily be sampled. From the systems studied here with nonzero α and β, we observe the formation of swarms over a wide range of Morse potential shapes, but for which the variational principle controlling structure formation is not simply minimization of a traditional (e.g., Helmholtz) free energy. In fact, the question of what general variational principles governing the behaviors of driven systems is a challenging and unanswered one [33]. Here we discuss how the swarms studied in this work are both similar to and different from structures formed via equilibrium self-assembly as a possible step towards answering this question.

The two most relevant driving forces for steady-state swarm formation are the balance of conservative forces between neighboring particles and the simultaneous achievement of the optimal velocity. All of the swarms we observe are made up of particles traveling at, or nearly at, v^*. In the case of ball swarms, these driving forces are relatively decoupled, with a potential energy minimizing structure that is stationary in reference frame moving at v^*. In the case of ring, shell, clumps, and tori the two driving forces are not so cleanly decoupled, and particles in these swarms have velocities that vary over time with averages near v^*. For these swarms with stationary centers of mass, the centripetal forces from particle rotation are balanced by the conservative forces between particles. It is straightforward to predict the size of the shell and ring swarms by equating these forces.

If these structures were emerging in nondissipative equilibrium systems we would expect structures with lower free energy (lower potential energy and higher entropy) to be more stable. Energetically, the ring and shell have nearly identical potential energy ($U_{\text{ring}} = -88010.46$, $U_{\text{shell}} = -88012.56$). Entropically, there are more ways to arrange particles on a shell than there are ways to arrange particles around a ring of the same diameter. Considering only the free energy of a swarm we would expect shells to be more stable than rings, which is inconsistent with our observation that rings never transform into shells. Perhaps there exists an "extended" free energy that can be written for self-propelled swarms that provides predictive capabilities. Previous work by Schweitzer *et al.* [21] provides a promising direction for such a development. The free energy would be extended in the sense that it adds additional nonequilibrium driving forces to a well-known equilibrium ensemble free energy. For the systems we study here, it seems natural that this extended free energy should include α, β, and γ, as these parameters provide the deviation from a standard equilibrium simulation. Because these terms describe the work put into the swarms and the dissipation of energy to the surrounding bath it follows that the free energy extension should incorporate dissipation.

Derivations for the functional form and demonstration of such an extended free energy are beyond the scope of the current work, but are an exciting challenge with important implications for theories of nonequilibrium self-assembly. Regions of parameter space in which structures coexist provide test cases for points at which extended free energies should equate, and therefore models such as the propelled Morse particles studied here are ideal candidates for theory development. The coexisting states in experimental systems such as in Ref. [6] can be used to compare and validate the theory.

V. CONCLUSIONS

We have performed extensive GPU-enabled simulations of self-propelled swarming particles, characterizing the structures that can be assembled over a wide range of parameters that tune the Morse interaction potential in three spatial dimensions. The diversity of the swarms stabilized in this system, their coexistence regions, and their sensitivity to thermal fluctuations (noise) highlights the need for efficient computer simulations with which parameter space can be explored and detailed experiments performed. We observe behaviors that are marked deviations from equilibrium self-assembly, including swarm coexistence and sensitivity to initial conditions, but our results suggest that modifications to equilibrium statistical mechanics approaches may have predictive capabilities. We propose a way forward, combining the swarms found in regions of coexistence as test cases for extended free energy development. Finally, the diversity of structures we observe here and the demonstrated control over their morphology may have immediate implications in the exploitation of swarms of practical interest.

ACKNOWLEDGMENTS

This work was supported by the Non-Equilibrium Energy Research Center (NERC), an Energy Frontier Research Center funded by the US Department of Energy, Office of Science, Office of Basic Energy Sciences under Award Number DE-SC0000989. E.J. received support from the James S. McDonnell Foundation 21st Century Science Research Award/Studying Complex Systems, grant no. 220020139, and from a National Defense Science and Engineering Graduate (NDSEG) Fellowship, 32 CFR 168a. N.N. also acknowledges the Vietnam Education Foundation. We thank Carolyn Phillips and Trung Dac Nguyen for helpful discussions and assistance, and Daphne Klotsa for comments on this manuscript.

[1] I. D. Couzin, J. Krause, R. James, G. D. Ruxton, and N. R. Franks, J. Theor. Biol. **218**, 1 (2002).
[2] T. Vicsek and A. Zafeiris, Physics Reports (2012).
[3] J. Toner and Y. Tu, Phys. Rev. E **58**, 4828 (1998).
[4] J. Toner, Y. Tu, and S. Ramaswamy, Ann. Phys. (NY) **318**, 170 (2005), special Issue.
[5] S. Hubbard, P. Babak, S. Sigurdsson, and K. Magnússon, Ecol. Model. **174**, 359 (2004).
[6] B. A. Grzybowski, H. A. Stone, and G. M. Whitesides, Nature (London) **405**, 1033 (2000).
[7] S. Chang, V. Paunov, D. Petsev, and O. Velev, Nat. Mater. **6**, 235 (2007).

[8] A. Baskaran and M. C. Marchetti, Phys. Rev. Lett. **101**, 268101 (2008).
[9] A. Baskaran and M. C. Marchetti, Phys. Rev. E **77**, 011920 (2008).
[10] S. Mishra, A. Baskaran, and M. C. Marchetti, Phys. Rev. E **81**, 061916 (2010).
[11] A. Baskaran and M. C. Marchetti, Proc. Natl. Acad. Sci. USA **106**, 15567 (2009).
[12] T. Vicsek, A. Czirók, E. Ben-Jacob, I. Cohen, and O. Shochet, Phys. Rev. Lett. **75**, 1226 (1995).
[13] A. Czirók, M. Vicsek, and T. Vicsek, Physica A **264**, 299 (1999).
[14] H. Levine, W.-J. Rappel, and I. Cohen, Phys. Rev. E **63**, 017101 (2000).
[15] G. Grégoire and H. Chaté, Phys. Rev. Lett. **92**, 025702 (2004).
[16] M. R. D'Orsogna, Y. L. Chuang, A. L. Bertozzi, and L. S. Chayes, Phys. Rev. Lett. **96**, 104302 (2006).
[17] C. András, H. E. Stanley, and V. Tamás, J. Phys. A **30**, 1375 (1997).
[18] A. Czirók and T. Vicsek, Physica A **281**, 17 (2000).
[19] A. Chetverikov, W. Ebeling, and M. Velarde, Eur. Phys. J. B **44**, 509 (2005).
[20] U. Erdmann, W. Ebeling, and A. Mikhailov, Phys. Rev. E **71**, 051904 (2005).
[21] F. Schweitzer, W. Ebeling, and B. Tilch, Phys. Rev. E **64**, 021110 (2001).
[22] J. R. Touma, A. Shreim, and L. I. Klushin, Phys. Rev. E **81**, 066106 (2010).
[23] Y.-L. Chuang, M. R. D'Orsogna, D. Marthaler, A. L. Bertozzi, and L. S. Chayes, Physica D **232**, 33 (2007).
[24] Y. Chuang, Y. Huang, M. D'Orsogna, and A. Bertozzi, in *Robotics and Automation, 2007 IEEE International Conference on* (IEEE, 2007), pp. 2292–2299.
[25] P. Ogren, E. Fiorelli, and N. Leonard, IEEE Trans. Automatic Control **49**, 1292 (2004).
[26] J. Strefler, U. Erdmann, and L. Schimansky-Geier, Phys. Rev. E **78**, 031927 (2008).
[27] http://codeblue.umich.edu/hoomd-blue/; J. A. Anderson, C. D. Lorenz, and A. Travesset, J. Comput. Phys. **227**, 5342 (2008).
[28] J. Deutch and I. Oppenheim, J. Chem. Phys. **54**, 3547 (1971).
[29] L. Verlet, Phys. Rev. **159**, 98 (1967).
[30] S. Plimpton, http://lammps.sandia.gov/.
[31] Y. Shi, L. Huang, and D. Brenner, J. Chem. Phys. **131**, 014705 (2009).
[32] See Supplemental Material at http://link.aps.org/supplemental/10.1103/PhysRevE.86.011136 for videos.
[33] M. Fialkowski, K. J. M. Bishop, R. Klajn, S. K. Smoukov, C. J. Campbell, and B. A. Grzybowski, J. Phys. Chem. B **110**, 2482 (2006).